Journal of Applied Fluid Mechanics, Vol. 12, No. 3, pp. 907-919, 2019.
Available online at www.jafmonline.net, ISSN 1735-3645, EISSN 1735-3645.
DOI: 10.29252/jafm.12.03.29180

Dynamic Responses of Sliding Isolation Concrete Liquid Storage Tank under Far-Field Long-Period Earthquake

W. Jing[1,2]† and X. Cheng[1,2]

[1] *Key Laboratory of Disaster Prevention and Mitigation in Civil Engineering of Gansu Province, Lanzhou University of Technology, Lanzhou, 730050, PR China*
[2] *Western Engineering Research Center of Disaster Mitigation in Civil Engineering of Ministry of Education, Lanzhou University of Technology, Lanzhou, 730050, PR China*

†Corresponding Author Email: jingwei3276@163.com

(Received May 9, 2018; accepted September 17, 2018)

ABSTRACT

Under far-field long-period earthquake, liquid storage tanks are easy to be failure because of large amplitude liquid sloshing. In this paper, nonlinear contact is used to simulate behavior of sliding isolation bearing, nonlinear dynamic equation is used to solve fluid-structure interaction, bilinear material model is used to simulate limiting-device, and 3-D calculation model of sliding isolation concrete rectangular liquid storage tank (CRLST) with limiting-devices is established. Firstly, artificial far-field long-period earthquake waves are synthesized based on the existing seismic records. Secondly, dynamic responses of sliding isolation CRLST under the action of short-period and far-field long-period earthquakes are studied. Thirdly, effects of bi-directional earthquake and structure size on dynamic responses are investigated. Lastly, displacement control measures are discussed. Results show that far-field long-period earthquakes mainly affect horizontal displacement of structure and liquid sloshing wave height, and sliding isolation has obvious control effect on liquid sloshing wave height. Besides, horizontal displacement of structure and liquid sloshing wave height are increased with increase of seismic dimension and structure size. The reasonable designs of sliding isolation bearing and limiting-device can solve the problem that the maximum horizontal displacement of sliding isolation CRLST may exceed the limit under far-field long-period earthquake.

Keywords: Sliding isolation; Concrete rectangular liquid storage tank (CRLST); Far-field long-period ground motion; Fluid-structure interaction; Liquid sloshing.

NOMENCLATURE

$A(\omega)$	fourier amplitude spectrum
$a(t)$	acceleration time history
a_0	seismic record acceleration
$a_g(t)$	non-stationary artificial ground motion
c	attenuation constant
$\mathbf{C}_{FF}$	damping matrix of liquid itself
$\mathbf{C}_{FU}$	damping matrix of liquid contributed by structure
$\mathbf{C}_{FU}$	damping matrix of structure contributed by liquid
$\mathbf{C}_{FU}$	stiffness matrix of structure contributed by liquid
$\mathbf{C}_{UU}$	damping matrix of structure itself
$f(t)$	non-stationary intensity envelope
$\mathbf{F}_F$	force caused by volume force
$\mathbf{F}_U$	force caused by liquid pressure
$(\mathbf{F}_F)_S$	force caused by area force
$I(\omega)$	imaginary parts of Fourier transform
$\mathbf{K}_{FF}$	stiffness matrix of liquid itself
$\mathbf{K}_{FU}$	stiffness matrix of liquid contributed by structure
$\mathbf{K}_{UU}$	stiffness matrix of structure itself
$\mathbf{M}_{FF}$	liquid mass matrix
$\mathbf{n}$	vector of internal normal direction
p	probability guarantee coefficient
PGA	peak ground acceleration
$R(\omega)$	real parts of Fourier transform
S	boundary of liquid domain
$S(\omega)$	power spectrum function
$S_a(\omega)$	target response spectrum

$S_a(T_i)$	spectral acceleration
$S_{ak}(\omega)$	maximum response spectrum
T_0	predominant period
T_d	duration of artificial seismic wave
T_d	seismic record duration
T_i	dispersion period
TOL	tolerance
T_r	mean period
$\mathbf{u}$	displacement vector
$\dot{\mathbf{u}}$	movement velocity
$\Delta\mathbf{u}$	unknown increment of displacement vector
V	liquid domain
ξ	damping ratio
ϕ	velocity potential
$\Delta\phi$	increment of velocity potential
β_l	weighted average
$\Delta\omega$	frequency interval
$\phi(\omega)$	phase spectrum
ϕ_k	initial phase spectrum

1. INTRODUCTION

Failure of concrete rectangular liquid storage tanks caused by earthquake will not only influence people's daily life and normal production of industrial enterprises, also will cause secondary disasters such as liquid leakage (Park *et al*. 2016; Hashimoto *et al*. 2017), fire and environmental pollution (Uckan *et al*. 2015), groundwater contamination issue (Dou *et al*. 2018a; 2018b), even more will threaten the lives of the people. Rubber isolation can reduce dynamic responses of liquid storage tanks, but which may increase liquid sloshing wave height (Calugatu and Mahin 2009); by comparison, sliding isolation will be better than rubber isolation (Shrimali and Jangid 2011).

There are many instances of destruction of oil storage tanks under long-period earthquakes. For example, in 1983, an earthquake (Ms=7.7) occurred in the central Japan Sea, liquid overflow of 13 liquid storage tanks was caused in Niigata city because of far-field long-period earthquake; meanwhile, the tank tops were also destroyed due to the impact force of liquid sloshing. In 1993, a large number of oil storage tanks located at Niigata Basin produced large amplitude liquid sloshing during Nanseioki earthquake, and the maximum wave height reached 1.7m. During the 2003 Tokachioki earthquake in Japan, 7 oil storage tanks located at Tomakomai were seriously damaged because of liquid sloshing (Zama 2004). In order to solve this problem, some researchers have been conducted. Matsui and Nagaya (2013) studied the nonlinear sloshing problem under long-period ground motion using finite element method. Shekari *et al.* (2010) investigated dynamic responses of isolated liquid storage tanks under long-period ground motion and found that dynamic responses corresponding to large and small height-diameter ratio were effectively controlled. Vakilazadsarabi (2015) found that destruction of liquid storage tank was related to liquid sloshing and studied the effects of long duration and long period resonant excitation on liquid sloshing response using nonlinear calculation method and experiment. Luo *et al*. (2015) found that dynamic responses of rubber isolation storage tank were effectively reduced under short-period ground motion, but under long-period ground motion, rubber isolation had no reduction effect on wave height.

In order to study dynamic responses of liquid storage tank, the corresponding simulation and model works is particularly important. Based on FSI, Shahverdiani *et al.* (2008) used finite element method to study dynamic responses of concrete liquid storage tank. Ozdemir *et al*. (2010) pointed out that numerical method was an indispensable and effective tool for evaluating the aseismic capability of liquid storage tank. Richter (2013) proposed a full Euler method for the FSI problem. Nicolici and Bilegan (2013) simulated the interaction between liquid and wall based on complete unidirectional coupling. Lay (2014) used finite element and boundary element methods to simulate structure and fluid domains, respectively, and then solved the coupling equation. Considering free surface liquid sloshing, Jing *et al*. (2018) and Cheng *et al*. (2017; 2018) studied the dynamic responses of CRLST by numerical simulation based on potential flow theory. Generally speaking, because numerical simulation method uses special element to simulate the liquid and FSI interface is treated more precisely, which can accurately reflect some particularities of liquid storage tank.

Many earthquake damage cases and research results shows that liquid sloshing is sensitive to far-field long-period ground motion, and it is necessary to study effect of long-period ground motion on design of liquid storage tank (Men *et al*. 2008; Zhou *et al.* 2012). At present, there is a lack of research on sliding isolation concrete liquid storage tanks under long-period ground motion. In this paper, the characteristics of far-field long-period ground motion are summarized firstly, and then the corresponding synthetic procedure is given. The mechanical behavior of sliding isolation is simulated by setting contact, and 3-D calculation model of sliding isolation concrete rectangular liquid storage tank (CRLST) with 8 limiting-devices is established considering nonlinear fluid-structure interaction (FSI). Dynamic responses of concrete rectangular liquid storage tank (CRLST) are studied comparatively under the action of short-period and far-field long-period ground motions, influences of far-field long-period ground motions on dynamic responses are evaluated, and effect of seismic response reduction of sliding isolation on CRLST is investigated under far-field long-period ground motion. Besides, in order to control structure displacement under far-field long-period ground motion, three control measures are proposed and their effectiveness is investigated. Lastly, some advices for the design and disaster prevention of sliding isolation concrete rectangular liquid storage tank (CRLST) under far-field long-period earthquake are provided.

2. FAR-FIELD LONG-PERIOD GROUND MOTION

2.1 Basic Concepts

Based on the analysis of San Fernando seismic records, Hanks (1975) first proposed the concept of long-period ground motion. After certain research and attention, starting from the Michoacan earthquake in 1985 and the Landers earthquake in 1992, the adverse effects of far-field long-period ground motion on long-period structure were gotten attention (Koketsu and Miyake 2008).

Some research results show that the characteristics of long-period ground motions are as follows: a) the larger the magnitude, the richer the longer period component; b) long-period component slowly decay with increase of epicenter distance; c) duration of long-period ground motions is long; d) thick cover layer has obvious amplification effect on the long-period component. So the main factors that affect the periodic characteristics of ground motions are site, epicentral distance, magnitude and source characteristics (Hu, 2006). With the deepening of the corresponding research, there are many clear definitions for the long-period ground motion, which are good to quantitatively describe the long-period ground motion. The details are as follows:

(1) Rathje *et al*. (1998) proposed the concept of mean period T_r and predominant period T_0 of the response spectrum based on the study of the spectral parameters of ground motion, and long-period ground motion is generally referred to as its predominant period T_0 is from several seconds to tens of seconds.

$$T_r = \frac{\sum_i T_i \left(\frac{S_a(T_i)}{PGA}\right)^2}{\sum_i \left(\frac{S_a(T_i)}{PGA}\right)^2}, \quad (0.02 \le T_i \le T) \tag{1}$$

$$T_0 = \frac{\sum_i T_i \ln\left(\frac{S_a(T_i)}{PGA}\right)}{\sum_i \ln\left(\frac{S_a(T_i)}{PGA}\right)} \tag{2}$$

where T_i is dispersion period with equal distance of acceleration response spectrum corresponding to 5% damping ratio; $S_a(T_i)$ is spectral acceleration corresponding to T_i; PGA is peak ground acceleration.

(2) In order to provide quantitative indicators for the selection of long-period ground motion, Li *et al*. (2014) defined weighted average β_l based on dynamic amplification factor spectrum curve, the curve from period 2s to 10s was selected. Based on the analysis of the existing seismic records, it was found that β_l of short-period ground motion was small, and β_l of far-field long-period ground motion was large. When β_l>0.4, the records were belong to the far-field long-period ground motions.

$$\beta_l = \frac{\sum T_i^2 \left(\frac{S_a(T_i)}{PGA}\right)}{\sum T_i^2} \tag{3}$$

where T_i is equal distance dispersion period of acceleration response spectrum with 5% damping ratio, its range of values is 2-10s; $S_a(T_i)$ is spectral acceleration corresponding to T_i; PGA is peak ground acceleration.

(3) If low frequency components of the seismic records are rich, namely, spectral components are mainly concentrated in 0.1-2Hz, then these records can be divided into long-period ground motions.

2.2 Artificial Synthesis of Far-Field Long-Period Ground Motion

The method of trigonometric series can be used to synthesize artificial seismic wave, the basic process is as follows:

(1) Obtaining the target response spectrum $S_a(\omega)$ by processing the existing far-field long-period seismic record.

(2) Converting the target response spectrum $S_a(\omega)$ to the power spectrum function $S(\omega)$:

$$S(\omega) \approx \frac{\xi}{\pi\omega} S_a^2(\omega) / \ln\left(-\frac{\pi}{\omega T_d} \ln p\right) \tag{4}$$

where ξ is damping ratio; ω is circular frequency; T_d is duration of artificial seismic wave; p is probability guarantee coefficient (≥0.85).

(3) Converting the power spectrum function $S(\omega)$ to the Fourier amplitude spectrum $A(\omega)$:

$$A(\omega) = \left[4S(\omega)\Delta\omega\right]^{1/2} \tag{5}$$

where $\Delta\omega$ is frequency interval, $\Delta\omega$=2π× sampling frequency /*FFT* length.

(4) Converting the natural seismic wave from time domain to frequency domain by Fourier transform, the phase spectrum $\phi(\omega)$ used for synthetic seismic wave can be obtained (Liao *et al*. 1992):

$$\begin{cases} R(\omega) + I(\omega) = \dfrac{1}{2\pi}\displaystyle\int_0^{T_d} a_0(t) e^{-j2\omega t} dt \\ \phi(\omega) = \arctan \dfrac{I(\omega)}{R(\omega)} \end{cases} \tag{6}$$

where $R(\omega)$ and $I(\omega)$ are the real and imaginary parts of Fourier transform of the existing record; T_d is duration of existing long-period seismic record; a_0 is acceleration of existing long-period seismic record.

(5) Converting Fourier amplitude spectrum $A(\omega)$ and phase spectrum $\phi(\omega)$ to the real and imaginary parts of Fourier transform, and the approximate acceleration time history $a(t)$ of artificial ground motion can be obtained by inverse Fourier transform:

$$a(t) = FFT^{-1}\left[A(\omega) e^{i\phi_k(\omega)}\right] \tag{7}$$

where ϕ_k is the initial phase spectrum.

(6) $a(t)$ is multiplied by non-stationary intensity envelope $f(t)$, then the acceleration time history $a_g(t)$ of non-stationary artificial ground motion can be obtained:

$$f(t) = \begin{cases} (t/T_1)^2; & 0 < t \le T_1 \\ 1; & T_1 < t \le T_2 \\ \exp\left[-c(t-T_2)\right]; & T_2 < t \le T_d \end{cases} \tag{8}$$

$$a_g(t) = a(t) f(t) \tag{9}$$

where c is attenuation constant, it is 0.1-1.0; the value of T_1 and T_2 can be decided according to the actual situation.

(7) Conducting Fourier transform for the acceleration time history $a_g(t)$ of non-stationary artificial ground motion. The maximum response spectrum $S_{ak}(\omega)$ corresponding to $a_g(t)$ at each frequency point can be obtained by convolution operation.

(8) Adjusting the Fourier amplitude spectrum $A(\omega)$ by the ratio of the target acceleration response spectrum $S_a(\omega)$ and the calculated response spectrum $S_{ak}(\omega)$:

$$A_{k+1}(\omega) = A_k(\omega) \frac{S_a(\omega)}{S_{ak}(\omega)} \tag{10}$$

(9) Repeating steps (2)-(8), when k=n, if the ratio of target acceleration response spectrum $S_a(\omega)$ to calculated response spectrum $S_{ak}(\omega)$ is close to 1.0, then loop end can be achieved.

$$TOL = \left|\frac{S_{ak}(\omega) - S_a(\omega)}{S_a(\omega)}\right| \tag{11}$$

ChiChi-CHY044 wave and TOM wave are used as the existing far-field long-period ground motions, and artificial wave 1 and artificial wave 2 are synthesized, respectively. Curves of acceleration response spectrum are shown in Figs. 1-2.

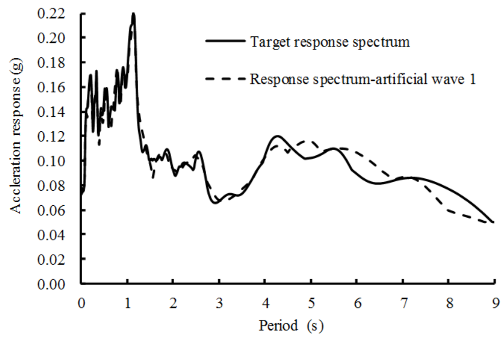

Fig. 1. Artificial wave 1.

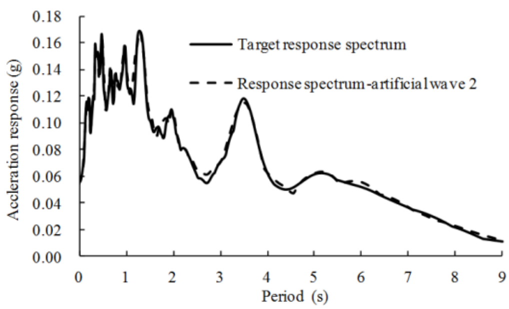

Fig. 2. Artificial wave 2.

3. THEORY OF FLUID-STRUCTURE INTERACTION

3.1 Motion Equation of Liquid Domain

Assuming that the unknown increment of velocity potential ϕ is $\Delta\phi$, the unknown increment of displacement vector **u** is Δ**u**, then the equation of motion in liquid domain can be expressed as:

$$\begin{bmatrix} 0 & 0 \\ 0 & -\mathbf{M}_{FF} \end{bmatrix}\begin{bmatrix} \Delta\ddot{\mathbf{u}} \\ \Delta\ddot{\phi} \end{bmatrix}+\begin{bmatrix} \mathbf{C}_{UU} & \mathbf{C}_{UF} \\ \mathbf{C}_{FU} & -\left(\mathbf{C}_{FF}+\left(\mathbf{C}_{FF}\right)_S\right) \end{bmatrix}\begin{bmatrix} \Delta\dot{\mathbf{u}} \\ \Delta\dot{\phi} \end{bmatrix}+ \begin{bmatrix} \mathbf{K}_{UU} & \mathbf{K}_{UF} \\ \mathbf{K}_{FU} & -\left(\mathbf{K}_{FF}+\left(\mathbf{K}_{FF}\right)_S\right) \end{bmatrix}\begin{bmatrix} \Delta\mathbf{u} \\ \Delta\phi \end{bmatrix}=\begin{bmatrix} 0 \\ 0 \end{bmatrix}-\begin{bmatrix} \mathbf{F}_U \\ \mathbf{F}_F+\left(\mathbf{F}_F\right)_S \end{bmatrix} \quad (12)$$

where $\mathbf{F}_U$, $\mathbf{F}_F$ and $(\mathbf{F}_F)_S$ are the force acting on structural boundary caused by liquid pressure, volume force and area force corresponding to liquid continuity equation; $\mathbf{M}_{FF}$ is liquid mass matrix; $\mathbf{C}_{UU}$, $\mathbf{C}_{FU}$, $\mathbf{C}_{UF}$ and $\mathbf{C}_{FF}$ are damping matrix of structure itself, damping matrix of liquid contributed by structure, damping matrix of structure contributed by liquid and damping matrix of liquid itself; $\mathbf{K}_{UU}$, $\mathbf{K}_{FU}$, $\mathbf{K}_{UF}$ and $\mathbf{K}_{FF}$ are stiffness matrix of structure itself, stiffness matrix of liquid contributed by structure, stiffness matrix of structure contributed by liquid and stiffness matrix of liquid itself.

$$\mathbf{F}_F=\int_V\left(\frac{\partial\rho}{\partial h}\dot{h}\delta\phi-\rho\nabla\phi\right)dV \quad (13)$$

$$\left(\mathbf{F}_F\right)_S=\int_S-\rho\dot{\mathbf{u}}\cdot\mathbf{n}\delta\phi dS \quad (14)$$

where V is liquid domain; S is boundary of liquid domain; **n** is vector of internal normal direction of S; $\dot{\mathbf{u}}$ is movement velocity of S.

A part of the liquid boundary surface S is assumed to be adjacent to the structure (Fig. 3), the boundary surface adjacent to the structure is represented as S_1, the force acting on structural boundary caused by liquid pressure $\mathbf{F}_U$ can be obtained by Eq. (15).

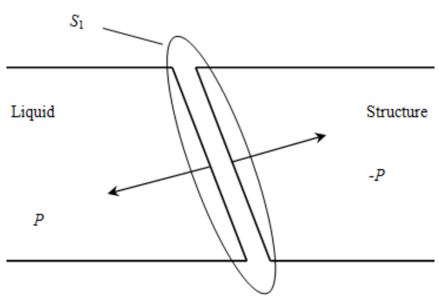

Fig. 3. Interaction of liquid and structure.

$$\begin{cases} -\delta F_U=-\int_{S_1} P\mathbf{n}\cdot\delta\mathbf{u}dS_1 \\ P=P(h)=P\begin{bmatrix} \Omega(\mathbf{x}+\mathbf{u})-\dot{\phi}- \\ \frac{1}{2}\mathbf{v}_n\cdot\mathbf{v}_n-\frac{1}{2}\mathbf{v}_t\cdot\mathbf{v}_t \end{bmatrix} \end{cases} \quad (15)$$

where $\mathbf{v}_n$ is liquid movement velocity perpendicular to the boundary, $\mathbf{v}_t$ is tangential velocity, P is liquid pressure.

$$\mathbf{v}_n=(\dot{\mathbf{u}}\cdot\mathbf{n})\mathbf{n} \quad \mathbf{v}_\tau=\nabla\phi-(\nabla\phi\cdot\mathbf{n})\mathbf{n} \quad (16)$$

3.1 FSI Equation

Because the system is non-linear, each exact solution needs multiple equilibrium iterations. Adding structure term into liquid motion Eq. (12), then the nonlinear FSI equation based on potential flow theory can be expressed as:

$$\begin{bmatrix} \mathbf{M}_{SS} & 0 \\ 0 & \mathbf{M}_{FF} \end{bmatrix}\begin{bmatrix} \Delta\ddot{\mathbf{u}} \\ \Delta\ddot{\phi} \end{bmatrix} +\begin{bmatrix} \mathbf{C}_{UU}+\mathbf{C}_{SS} & \mathbf{C}_{UF} \\ \mathbf{C}_{FU} & -\left(\mathbf{C}_{FF}+\left(\mathbf{C}_{FF}\right)_S\right) \end{bmatrix}\begin{bmatrix} \Delta\dot{\mathbf{u}} \\ \Delta\dot{\phi} \end{bmatrix}+ \begin{bmatrix} \mathbf{K}_{UU}+\mathbf{K}_{SS} & \mathbf{K}_{FU} \\ \mathbf{K}_{UF} & -\left(\mathbf{K}_{FF}+\left(\mathbf{K}_{FF}\right)_S\right) \end{bmatrix} \begin{bmatrix} \Delta\mathbf{u} \\ \Delta\phi \end{bmatrix}=\begin{bmatrix} \mathbf{F}_{SS} \\ 0 \end{bmatrix}-\begin{bmatrix} \mathbf{F}_U \\ \mathbf{F}_F+\left(\mathbf{F}_F\right)_S \end{bmatrix} \quad (17)$$

where $\mathbf{M}_{SS}$, $\mathbf{C}_{SS}$ and $\mathbf{K}_{SS}$ are mass, damping and stiffness matrix of structure; $\mathbf{F}_{SS}$ is load vector acting on structure.

4. NUMERICAL EXAMPLE

4.1 Calculation Model

The length, width and height of concrete rectangular liquid storage tank (CRLST) is 6m×6m×4.8m (Cheng *et al*. 2017; 2018) or 12m×6m×4.8m, the wall thickness is 0.3m. Assuming the concrete material is elastic, its density is 2500kg/m^3, its elastic modulus is 3×10^{10}Pa, and its Poisson's ratio is 0.2. Liquid level height is 3.6m, liquid density is 1000kg/m^3, and the bulk modulus is 2.3×10^{9}Pa. 8 limiting-devices are arranged at the bottom of the rectangular liquid-storage structure, bilinear material model and Beam element are used for these limiting-devices, material parameters of limiting-device are shown in Table 1 (Cheng *et al*. 2017). 3-D Solid element is used to simulate structure and 3-D Fluid element is used to simulate liquid.

Nonlinear contact surface is set to simulate the behavior the sliding isolation layer. Schematic diagram of connection of limiting-device is shown in Fig. 4, and the corresponding calculation models established by ADINA 9.0 are shown in Fig. 5.

Table 1 Material parameters of limiting-device

Elastic modulus *E*/Pa	Poisson's ratio ν	Yield strength σ/MPa	Density ρ/kg/m^3	Strain hardening modulus *E*/Pa	Yield strain ε	Maximum plastic strain ε_u
2×10^{11}	0.3	235	7800	2×10^{9}	0.001	0.02

Table 2 Earthquake information

Short-period ground motions			Far-field long-period ground motions		
Name	Station	Date	Name	Station	Date
El-Centro	--	1940/5/18	ChiChi	CHY044	1999/9/20
Imperial Valley	USGS 5115	1979/10/15	ChiChi	TCU052	1999/9/20
Loma Prieta	090 CDMG 47381	1989/10/18	ChiChi	TCU115	1999/9/20
Trinidad	090 CDMG 1498	1983/8/24	TOM	Tomakomai K-NET	2003/9/26
Hollister	USGS 1028	1961/4/9	Synthetic wave 1	--	--
Northridge	090 CDMG 24278	1994/1/17	Synthetic wave 2	--	--

Table 3 Predominant period of ground motion

Short-period ground motion	Predominant period /s	Long-period ground motion	Predominant period /s
El-Centro	0.56	ChiChi-CHY044	1.28
Friuli	0.26	HWA013	1.44
Imperial	0.14	ChiChi-TCU052	1.08
Loma	0.22	ChiChi-TCU115	2.22
Trinidad	0.28	TOM	1.14
Hollister	0.38	Artificial wave 1	1.14
Northridge	0.26	Artificial wave 2	1.30

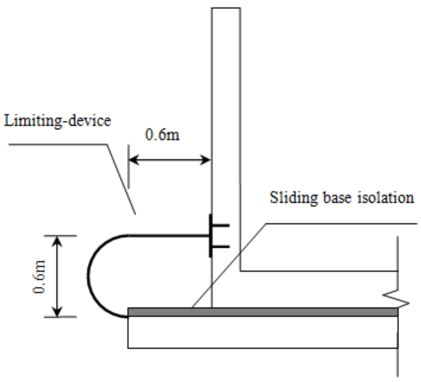

Fig. 4. Schematic diagram of connection of limiting-device.

4.2 Ground Motion Selection

In order to study effect of far-field long-period ground motion on dynamic responses of sliding isolation concrete rectangular liquid storage tank (CRLST), 6 short-period ground motions and 6 far-field long-period ground motions (4 natural ground motions and 2 synthetic waves) are selected, and the details are shown in Table 2. Acceleration, acceleration response spectra, Fourier spectra and power spectra of far-field long-period ground motion (TOM) and short-period ground motion (El-Centro) are shown in Fig. 6. Predominant periods of the selected waves are shown in Table 3.

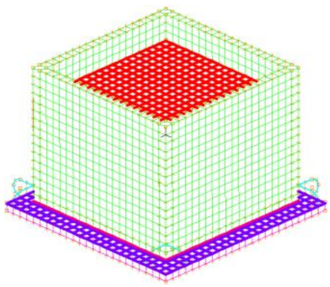

(a) 6m×6m×4.8m

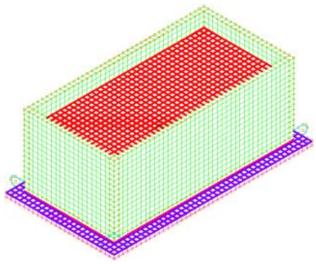

(a) 12m×6m×4.8m

Fig. 5. Calculation models.

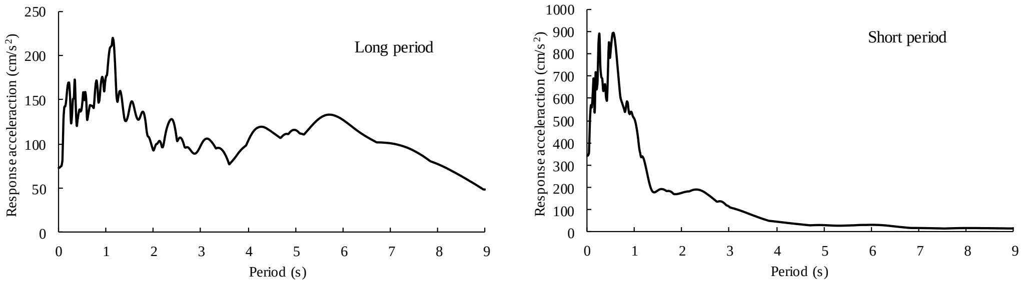

(a) Acceleration response spectra

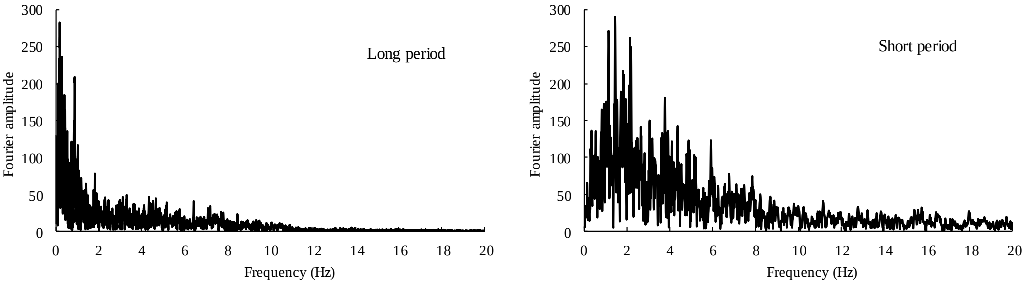

(b) Fourier spectra

Fig. 6. Comparison of far-field long-period and short-period ground motions.

Table 4 Maximum horizontal displacement/mm

Short-period earthquakes	El-Centro	Imperial-Valley	Loma-Prieta	Trinidad	Hollister	Northridge
	11.571	7.643	9.697	4.321	8.257	5.100
Far-field long-period earthquakes	CHY044	TCU052	TCU115	TOM	Artificial wave 1	Artificial wave 2
	60.988	60.226	100.949	53.483	79.484	84.900

Table 5 Maximum wave height/m

Short-period earthquakes	El-Centro	Imperial-Valley	Loma-Prieta	Trinidad	Hollister	Northridge
	0.186	0.166	0.186	0.023	0.045	0.013
Far-field long-period earthquakes	CHY044	TCU052	TCU115	TOM	Artificial wave 1	Artificial wave 2
	0.398	0.511	0.588	0.420	0.314	0.391

As shown in Fig. 6, compared with the short-period ground motion, the duration of far-field long-period ground motion is longer, and the acceleration response spectrum decays slowly with increase of period, the Fourier spectrum is mainly distributed in the range of 0-1.0Hz. As shown in Table 3, the predominant period of far-field long-period ground motion is obviously larger than that of short-period ground motion. Besides, the predominant period of artificial wave are also longer, so the feasibility that long-period artificial wave can be synthesized with the help of existing far-field long-period wave can be proved. In summary, duration, acceleration response spectrum, Fourier spectrum, Power spectrum and predominant period can be comprehensively used to judge whether one record is belong to far-field long-period ground motion.

4.3 Effect of Far-Field Long-Period Earthquake on Dynamic Responses

Because the amplitude of far-field long-period ground motion is generally small, the PGAs of the selected ground motions are adjusted to 0.22g. For concrete rectangular liquid storage tank (CRLST), the most important two types of failure modes are liquid overflow and wall cracking. After the sliding isolation measures being taken, the pipeline destruction due to excessive horizontal

Table 6 Maximum wall tension stress/MPa

Short-period earthquakes	El-Centro	Imperial-Valley	Loma-Prieta	Trinidad	Hollister	Northridge
	1.445	1.500	1.446	1.306	1.390	1.389
Far-field long-period earthquakes	CHY044	TCU052	TCU115	TOM	Artificial wave 1	Artificial wave 2
	0.975	0.958	0.970	0.988	0.984	0.956

Table 7 Maximum liquid pressure/kPa

Short-period earthquakes	El-Centro	Imperial-Valley	Loma-Prieta	Trinidad	Hollister	Northridge
	63.253	60.722	68.681	66.381	69.479	66.314
Far-field long-period earthquakes	CHY044	TCU052	TCU115	TOM	Artificial wave 1	Artificial wave 2
	46.204	45.345	41.955	41.827	43.584	43.090

Table 8 Isolation effect on wave height/m

Far-field long-period earthquakes	CHY044	TCU052	TCU115	TOM	Artificial wave 1	Artificial wave 2
No-isolation liquid storage tank	0.665	0.810	0.878	0.754	0.524	0.682
Isolation liquid storage tank	0.398	0.511	0.588	0.420	0.314	0.391
Damping coefficient	0.401	0.369	0.330	0.443	0.401	0.427

displacement will also be a failure mode. Besides, liquid pressure is also an important problem in the study of liquid storage tank. Therefore, the effect of far-field long-period earthquakes on the maximum horizontal displacement, the maximum wave height, the maximum wall tension stress and the maximum liquid pressure should be focused on research, and the specific calculation results are shown in Table 4, Table 5, Table 6, and Table 7.

As shown in Table 4, Table 5, Table 6 and Table 7, although the amplitude of PGA of far-field long-period ground motion is relatively small, the horizontal displacement and the wave height caused by this kind of ground motion is much greater than that of the short-period ground motion. On the contrary, the wall tension stress caused by far-field long-period ground motion is smaller than that of short-period ground motion, and the wall tension stress corresponding to the far-field long-period ground motion is far less than the tensile strength of concrete, so the occurrence probability of wall cracking under far-field long-period earthquake is small after sliding isolation being taken. Besides, the liquid pressure caused by far-field long-period ground motion is obviously smaller than that of short-period ground motion. It can be seen that far-field long-period ground motion mainly affects the displacement responses (horizontal displacement and wave height) of sliding isolation concrete rectangular liquid storage tank (CRLST), so the main failure modes of sliding isolation concrete rectangular liquid storage tank (CRLST) under the action of far-field long-period earthquake may be excessive horizontal displacement and liquid overflow.

4.4 Analysis of Seismic Isolation Effect

From the analysis of Section 4.3, wall tensile stress is small under far-field long-period ground motion, but wave height is large, which is easy to cause the occurrence of liquid overflow. Under the action of far-field long-period ground motion, it is necessary to investigate the control effect of sliding isolation on wave height. The maximum wave heights corresponding to no-isolation and isolation liquid storage tank are shown in Table 8.

As shown in Table 8, sliding isolation has certain control effect on wave height; on the contrary, the existing research results have shown that the commonly used rubber isolation had amplification effect on wave height under the action of far-field long-period ground motion (Luo *et al*. 2015). Because the amplitude of far-field long-period ground motion is small, the dynamic responses of structure are generally small, and sliding isolation effect on liquid storage tank can be reflected by the reduction of wave height. Compared with rubber isolation, sliding isolation has more important meaning for disaster control of concrete rectangular liquid storage tank (CRLST) under the action of far-field long-period ground motion. The control mechanism of sliding isolation for wave height needs to be further studied in the future under the action of far-field long-period ground motion.

Table 9 Effect of bi-directional earthquake on horizontal displacement/mm

Far-field long-period earthquakes	CHY044	TCU052	TCU115	TOM	Artificial wave 1	Artificial wave 2
Unidirectional	60.988	60.226	100.949	53.483	79.484	84.900
Bi-directional	70.051	77.014	141.983	55.187	95.429	124.249

Table 10 Effect of bi-directional far-field long-period earthquake on wave height/m

Far-field long-period earthquakes	CHY044	TCU052	TCU115	TOM	Artificial wave 1	Artificial wave 2
Unidirectional	0.398	0.511	0.588	0.420	0.314	0.391
Bi-directional	0.795	0.952	1.120	0.749	0.622	0.744

Table 11 Effect of structural size on horizontal displacement/mm

Far-field long-period earthquakes	CHY044	TCU052	TCU115	TOM	Artificial wave 1	Artificial wave 2
6m×6m×4.8m	60.988	60.226	100.949	53.483	79.484	84.900
12m×6m×4.8m	96.856	351.792	281.161	524.317	124.737	408.847

Table 12 Effect of structural size on wave height/m

Far-field long-period earthquakes	CHY044	TCU052	TCU115	TOM	Artificial wave 1	Artificial wave 2
6m×6m×4.8m	0.398	0.511	0.588	0.420	0.314	0.391
12m×6m×4.8m	0.575	0.601	0.958	0.779	0.602	0.690

4.5 Effect of Bi-directional Earthquake on Dynamic Responses

The sliding isolation system could behave differently under bi-directional earthquake, so it is necessary to study dynamic responses of sliding isolation concrete rectangular liquid storage tank (CRLST) under bidirectional far-field long-period seismic action. The ratio of PGA in *x*-axis direction and *y*-direction is adjusted to 1:0.85. It is obtained that far-field long-period ground motion mainly affects structure displacement responses of the system through the above analysis, so the influences of bi-directional far-field long-period earthquake actions on the structure displacement and liquid sloshing wave height are listed in Tables 9 and 10.

As shown in Tables 9 and 10, the maximum structure displacement and liquid wave height are obviously increased after bi-directional far-field long-period seismic action being considered. For example, under bidirectional ChiChi-TCU115 earthquake action, the structural displacement is increased by 40.65%; while under the 5 far-field long-period earthquake action, liquid sloshing wave height is amplified about 2 times. Thus, in the research and application of sliding isolation concrete rectangular liquid storage tank (CRLST) under far-field long-period earthquake action, in order to get more reasonable results and improve structure safety, effect of horizontally bi-directional far-field long-period earthquake action should be considered.

4.6 Effect of Structure Size on Dynamic Responses

In order to study the influence of structural size on the sliding isolation concrete rectangular liquid storage tank (CRLST), two sizes 6m×6m×4.8m and 12m×6m×4.8m are selected, for the latter, ground motion is input along the long axis direction. The maximum horizontal displacement and the maximum wave height corresponding to the two sizes are listed in Table 11 and Table 12.

As shown in Tables 11 and 12, the maximum horizontal displacement increases with the increase of structural size, and when the designs of friction coefficient and limiting-device are unreasonable, it is easy to produce the problem of excessive horizontal displacement. The maximum wave height also increases with the increase of structural size, when the structural size is 12m×6m×4.8m, the maximum wave height of sliding isolation liquid storage tank reaches 0.958m under the action of ChiChi-TCU115 earthquake, if the reserved no-liquid wall height is not enough, it is easy to cause liquid overflow. It can be seen that the larger the structure is, the effect of far-field long-period ground motion on displacement and wave height will be more significant.

4.7 Control Measures of Horizontal Displacement

Based on the above analysis, maximum horizontal displacement of sliding isolation concrete rectangular liquid storage tank (CRLST) increases with the increase of structure size. When the designs of friction coefficient and the limiting-device are unreasonable, the horizontal displacement is easy to exceed the limit. As shown in Table 8, horizontal displacement of concrete rectangular liquid storage tank with size of 12m×6m×4.8m are the largest, its value is 524.317mm, which has affected the effectiveness of sliding isolation structure. Therefore, the displacement control measure under the action of TOM wave is taken as an example.

4.7.1 Measure I- Adjusting Friction Coefficient

Friction coefficient is an important design parameter, which not only directly affects the effect of shock absorption, but also has a great effect on the horizontal displacement. The variation law of the maximum horizontal displacement when the friction coefficient is 0.02, 0.04, 0.06 and 0.08 is shown in Fig. 7.

As shown in Fig. 7, when the diameter of limiting-device is constantly equal to 7 cm, the maximum horizontal displacement of structure decreases with the increase of friction coefficient, but when the friction coefficient is 0.06, the horizontal displacement is still larger. Although the horizontal displacement can be reduced by further increasing the friction coefficient, the reduction effect of sliding isolation on liquid storage tank will be weakened. Therefore, controlling the horizontal displacement by only changing the friction coefficient is not enough.

4.7.2 Measure II- Adjusting Diameter of Limiting-Device

The diameter of limiting-device can affect the stiffness of isolation layer. In order to discuss the control effect of the limiting-device on the horizontal displacement, it is assumed that the diameters of limiting-device are 7cm, 8cm, 9cm and 10cm, respectively. Effect of measure II on horizontal displacement is shown in Fig. 8.

As shown in Fig. 8, when the coefficient of friction is constantly equal to 0.02, increasing the diameter of limiting-device can effectively control the horizontal displacement of structure. When the diameter of limiting-device is 10cm, the maximum horizontal displacement can be controlled within the scope of the requirements. However, if the diameter of the limiting-device is too large, the stiffness of the isolation layer will be great, as a result, the structure motion under the action of some earthquakes will be greatly restricted, so as to reduce the use range of isolation effect.

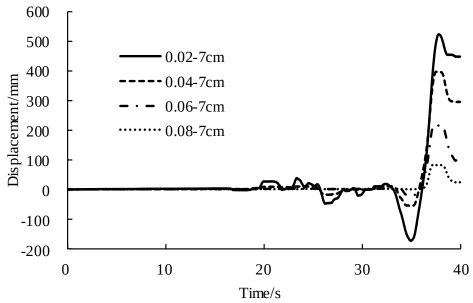

Fig. 7. Effect of measure I on horizontal displacement.

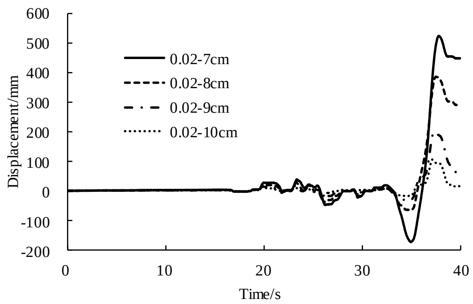

Fig. 8. Effect of measure II on horizontal displacement.

4.7.3 Measure III- Adjusting Friction Coefficient and Diameter of Limiting-Device Simultaneously

There are certain defects when only measure I or measure II is taken to achieve the displacement control, so it is necessary to study the control effect on displacement when the measures I and II are taken simultaneously. The friction coefficient is increased from 0.02 to 0.04, 0.06 and 0.08; the diameter of limiting-device is increased from 7cm to 8cm, 9cm and 10 cm. The effect of measure III on the horizontal displacement of structure is shown in Fig. 9.

As shown in Fig. 9, the horizontal displacement can be significantly reduced by increasing the friction coefficient and the diameter of limiting-device at the same time. Smaller friction coefficient can be selected, it is good to give full play to the advantage of sliding isolation for concrete rectangular liquid storage tank (CRLST); besides, the diameter of limiting-device can be designed to be smaller, the structure can still move under the action of some small earthquakes. Therefore, adjusting the friction

Table 13 Effect of control measure on maximum horizontal displacement of structure

Measure I	Displacement/mm	Measure II	Displacement/mm	Measure III	Displacement/mm
0.02-7cm	524.317	0.02-7cm	524.317mm	0.02-7cm	524.317mm
0.04-7cm	397.756	0.02-8cm	386.069mm	0.04-8cm	216.776mm
0.06-7cm	216.407	0.02-9cm	199.769mm	0.06-9cm	**54.154mm**
0.08-7cm	**83.481**	0.02-10cm	**105.544mm**	0.08-10cm	19.364mm

Table 14 Effect of control measure on maximum wave height

Measure I	Wave height/m	Measure II	Wave height/m	Measure III	Wave height/m
0.02-7cm	0.779m	0.02-7cm	0.779m	0.02-7cm	0.779m
0.04-7cm	0.995m	0.02-8cm	0.963m	0.04-8cm	1.093m
0.06-7cm	1.104m	0.02-9cm	1.125m	0.06-9cm	**1.173m**
0.08-7cm	**1.177m**	0.02-10cm	**1.161m**	0.08-10cm	1.183m

coefficient and the diameter of limiting-device at the same time is an effective method to control horizontal displacement of sliding isolation concrete rectangular liquid storage tank (CRLST) under the action of far-field long-period ground motion.

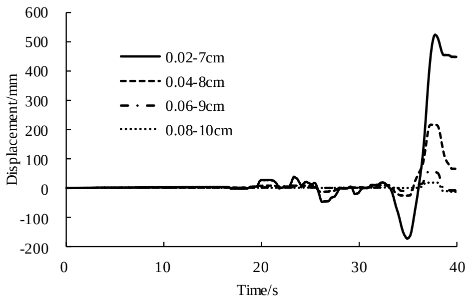

Fig. 9. Effect of measure III on horizontal displacement.

4.8 Effects of Control Measures on Maximum Horizontal Displacement and Wave Height

In order to study the effects of displacement control measures on the system response, and provide reference for engineering application, the maximum horizontal displacement of structure and wave height corresponding to different displacement control measures are listed in Tables 13 and 14.

As shown in Table 13, purely from the point of view of displacement control, the three control measures are all effective, effect of measure III on displacement control is best, measure I is the second, measure II is the third. Comparing Tables 13 and 14, it is found that as the displacement decreases, the wave height of the liquid increases. If the displacement limit 150mm proposed in the literature (Cheng *et al.*, 2017) is used as the control target, when friction coefficient is 0.08 and diameter of limiting-device is 7cm, the maximum displacement of the structure corresponding to measure I is 83.481mm, which meets the requirement, in this case, the maximum liquid wave height is 1.177m; when friction coefficient is 0.02 and diameter of limiting-device is 10cm, the maximum displacement of the structure corresponding to measure II is 105.544mm, which meets the requirement, in this case, the maximum liquid wave height is 1.161m; when friction coefficient is 0.06 and diameter of limiting-device is 9cm, the maximum displacement of the structure corresponding to measure III is 54.154mm, which meets the requirement, in this case, the maximum liquid wave height is 1.173m. On the whole, on the premise that the three types of control measures make the structural displacement meet the requirement, the wave height difference is small, so measures III are relatively best for displacement control of sliding isolation concrete rectangular liquid storage tank (CRLST) under far-field long-period earthquake.

5. CONCLUSIONS

(1) Artificial far-field long-period ground motion can be synthesized with the help of the existing far-field long period earthquake records, and the artificial wave can reflect the characteristics of far-field long-period ground motion, which can provide convenience for time history analysis of engineering structure.

(2) Wave height is sensitive to far-field long-period ground motion, and far-field long-period ground motion will cause large wave height, so the risk of liquid overflow will be increased. Fortunately, the sliding isolation has certain reduction effect on wave height.

(3) Large horizontal displacement of concrete rectangular liquid storage tank (CRLST) will be caused under the action of far-field long-period ground motion. Adjusting the friction coefficient and the limiting-device synthetically, the horizontal displacement of

sliding isolation concrete rectangular liquid storage tank (CRLST) could be effectively controlled.

(4) Horizontally bidirectional far-field long-period earthquake actions can further increase the horizontal displacement of structure and liquid wave height; the larger the structural size, horizontal displacement and wave height of concrete rectangular liquid storage tank (CRLST) will be larger.

(5) Far-field long-period earthquake has a great influence on the displacement responses of the system, in order to improve the effectiveness of sliding isolation concrete rectangular liquid storage tank (CRLST) under the action of far-field long-period ground motion, it should be paid attention to the control of horizontal displacement and wave height, then the reasonable design of sliding isolation concrete rectangular liquid storage tank (CRLST) can be achieved.

(6) The FSI method adopted in this paper can not consider the non-linearity of liquid sloshing completely and truly, in order to study the dynamic responses of concrete rectangular liquid storage tank (CRLST) more truly, it is necessary to simulate the sloshing behavior of liquid more reasonably based on discrete element method in future work.

ACKNOWLEDGMENTS

This paper is a part of the China Postdoctoral Science Foundation (2018M633652XB), and a part of the National Natural Science Foundation of China (Grant number: 51368039, 51478212), and a part of the Education Ministry Doctoral Tutor Foundation of China (Grant number: 20136201110003), and a part of the Plan Project of Science and Technology in Gansu Province (Grant number: 144GKCA032).

REFERENCES

Calugaru, V. and S. A. Mahin (2009). Experimental and analytical studies of fixed base and seismically isolated liquid storage tanks. *Proceedings of the 3rd International Conference on Advances in Experimental Structural Engineering*, San Francisco, CA 16, 1-12.

Cheng, X. S., W. Jing and L. J. Gong (2017). Simplified model and energy dissipation characteristics of a rectangular liquid-storage structure controlled with sliding base isolation and displacement-limiting devices. *Journal of Performance of Constructed Facilities, ASCE* 31(5), 1-11.

Cheng, X. S., W. Jing and L. J. Gong (2018). Dynamic responses of a sliding base-isolated RLSS considering free surface liquid sloshing. *KSCE Journal of Civil Engineering* 1-13.

Dou, Z., Chen, Z., Zhou, Z. *et al*. (2018a). Influence of eddies on conservative solute transport through a 2D single self-affine fracture. *International Journal of Heat & Mass Transfer* 121, 597-606.

Dou, Z., Zhou, Z., Wang, J. *et al*. (2018b). Roughness scale dependence of the relationship between tracer longitudinal dispersion and Peclet number in variable-aperture fractures. *Hydrological Processes* 32(10), 1461-1475.

Hanks, T. C. (1975). Strong ground motion of the San Fernando, California, earthquake: ground displacements. *Bulletin of the Seismological Society of America* 65(1), 193-225.

Hashimoto, H., Y. Hata and K. Kawamura (2017). Estimation of oil overflow due to sloshing from oil storage tanks subjected to a possible Nankai Trough earthquake in Osaka bay area. *Journal of Loss Prevention in the Process Industries* 50, 337-346.

Hu, L. X. (2006). Earthquake engineering. *Beijing: Seismological Press* 104-109. (in Chinese)

Jing, W., X. S. Cheng and W. Shi (2018). Dynamic responses of sliding isolation concrete rectangular liquid storage structure with limiting-devices under bidirectional earthquake actions. *Arabian Journal for Science and Engineering* 43, 1911-1924.

Koketsu, K. and H. Miyake (2008). A seismological overview of long-period ground motion. *Journal of Seismology* 12(2), 133-143.

Lay, K. S. (2014). Seismic coupled modeling of axisymmetric tanks containing liquid. *American Society of Civil Engineers* 119(9), 1747-1761.

Li, X. H., W. K. Wang, D. Wu, X. L. Xu, Z. J. Li and Y. X. Li (2014). The bounded method and characteristics analysis for long-period ground motions. *Journal of Vibration Engineering* 27(5), 685-692.

Liao, X. D. and J. Y. Su (1992). Study on artificial seismic waves with natural seismic characteristics. *Earthquake Engineering* 29(4), 33-36.

Luo, D. Y., J. G. Sun, J. F. Hao, Z. Wang and L. F. Cui (2015). The effect analysis of the LNG storage tanks with pile foundation and base isolation under the long period earthquake. *Earthquake engineering and Engineering Vibration* 35(6), 170-176.

Matsui, T. and T. Nagaya (2013). Nonlinear sloshing in a floating-roofed oil storage tank under long-period seismic ground motion. *Earthquake Engineering & Structural Dynamics* 42(7), 973-991.

Men, J. J., Q. X. Shi and X. H. Chen (2008). Seismic damage of high buildings caused in the remote areas from epicenter and aseismic design suggestion. *Journal of Xi'an University of Architecture & Technology (Natural Science Edition)* 40(5), 648-653.

Nicolici, S. and R. M. Bilegan (2013). Fluid structure interaction modeling of liquid sloshing phenomena in flexible tanks. *Nuclear Engineering & Design* 258(2), 51-56.

Ozdemir, Z., M. Souli and Y. M. Fahjan (2010). Application of nonlinear fluid-structure interaction methods to seismic analysis of anchored and unanchored tanks. *Engineering Structures* 32(2), 409-423.

Park, J. H., D. Bae and K. O. Chang (2016). Experimental study on the dynamic behavior of a cylindrical liquid storage tank subjected to seismic excitation. *International Journal of Steel Structures* 16(3), 935-945.

Rathje, E. M., N. A. Abrahamson and J. D. Bray (1998). Simplified frequency content estimates of earthquake ground motions. *Journal of Geotechnical & Geoenvironmental Engineering* 124(2), 150-159.

Richter, T. (2013). A Fully Eulerian formulation for fluid-structure-interaction problems. *Journal of Computational Physics* 233(2), 227-240.

Shahverdiani, K., A. R. Rahai and F. Khoshnoudian (2008). Fluid-structure interaction in concrete cylindrical tanks under harmonic excitations. *International Journal of Civil Engineering* 6(2), 132-141.

Shekari, M. R., N. Khaji and M. T. Ahmadi (2010). On the seismic behavior of cylindrical base-isolated liquid storage tanks excited by long-period ground motions. *Soil Dynamics & Earthquake Engineering* 30(10), 968-980.

Shrimali, M. K. and R. S. Jangid (2011). A comparative study of performance of various isolation systems for liquid storage tanks. *International Journal of Structural Stability & Dynamics* 2(4), 573-591.

Uckan, E., Önder, U., Uncu, G. *et al*. (2015). Seismic response of base isolated liquid storage tanks to near fault pulse type ground motions. *3rd Turkish Conference on Earthquake Engineering and Seismology*, October 14-16, Izmir/Turkey.

Vakilazadsarabi, A. (2015). Sloshing phenomena in tanks due to long period-long duration harmonic motions. *International Journal of Engineering Science & Technology* 7(3), 148-160.

Zama, S. (2004). Seismic hazard assessment for liquid sloshing of oil storage tanks due to long-period strong ground motions in Japan. *Proceedings of the 13th World Conference on Earthquake Engineering*.

Zhou, F. L., Cui, H. C., Shigetaka, A. B. E., *et al*. (2012). Inspection report of the disaster of the East Japan earthquake by Sino-Japanese joint mission. *Building Structure* 42(4), 1-20.